Results in Engineering 24 (2024) 103216

Contents lists available at ScienceDirect

Results in Engineering

journal homepage: www.sciencedirect.com/journal/results-in-engineering

Research paper

Performance improvement of THz MIMO antenna with graphene and prediction bandwidth through machine learning analysis for 6G application

Md Ashraful Haque [a], Redwan A. Ananta [a], Jamal Hossain Nirob [a], Md. Sharif Ahammed [a], Narinderjit Singh Sawaran Singh [b], Liton Chandra Paul [c], Abeer D. Algarni [d], Mohammed ElAffendi [e], Abdelhamied A Ateya [e,f,*]

[a] Department of Electrical and Electronic Engineering, Daffodil International University, Dhaka, 1207, Bangladesh
[b] Faculty of Data Science and Information Technology, INTI International Universitya, Persiaran Perdana BBN, Nilai, 71800, Negeri Sembilan, Malaysia
[c] Department of Electrical, Electronic and Communication Engineering, Pabna University of Science and Technology, Pabna, Bangladesh
[d] Department of Information Technology, College of Computer and Information Sciences, Princess Nourah bint Abdulrahman University, P.O. Box 84428, Riyadh, 11671, Saudi Arabia
[e] EIAS Data Science Lab, College of Computer and Information Sciences, Prince Sultan University, Riyadh, 11586, Saudi Arabia
[f] Department of Electronics and Communications Engineering, Zagazig University, Zagazig, 44519, Egypt

ARTICLE INFO

Keywords:
THz
MIMO
6G
Machine learning
RLC

ABSTRACT

This article provides the findings of a study that integrated simulation, an RLC equivalent circuit, and machine learning (ML) techniques to improve wireless indoor communications clusters with future 6 G applications. The antenna being presented is constructed on a polyimide substrate. It exhibits an isolation of 27 dB and has a bandwidth of 4.331 THz, ranging from 0.631 THz to 4.962 THz. Along with its small size (95.52 × 227.24) μm^2, it boasts an impressive maximum gain of 13.3 dB and an efficiency rating of 95 %. The ECC value drops below 0.0002 when the DG goes over 9.99. An advanced design system (ADS) creates a model like the proposed MIMO antenna to compare the return loss caused by CST (Computer Simulation Technology). Subsequently, following extensive data sampling with CST MWS (Microwave Studio) simulation, we employed supervised regression ML techniques. Gaussian process regression demonstrates exceptional accuracy, reaching almost 99 %, as evidenced by the high R-square and var scores. Additionally, it achieves the lowest error, less than one, while predicting bandwidth. The proposed antenna demonstrates strong potential as a formidable contender for 6 G THz band applications, as evidenced by the outcomes of the CST simulations and the prognostications derived from the machine learning techniques.

1. Introduction

The growing need for high data speeds and minimal latency is pushing the development of next-generation wireless communication systems towards the terahertz (THz) frequency range. These systems, particularly for 6 G, offer exceptional connectivity, enabling various applications such as holographic communications, ultra-reliable low-latency networks, and extensive Internet of Things (IoT) implementations [1]. Multiple-input and multiple-output (MIMO) antenna systems have emerged as crucial technologies to meet these demands. MIMO antennas enhance data speeds, spectrum efficiency, and signal stability by using multiple antennas for simultaneous transmission and reception [2]. However, traditional materials and designs face significant challenges at THz frequencies due to high losses, limited bandwidth, and inefficient propagation. Graphene, a two-dimensional material with outstanding electrical and mechanical properties, provides a promising solution to address these challenges [3]. Graphene's tunable conductivity, high electron mobility, and ability to support surface plasmon polaritons at terahertz frequencies make it an ideal candidate for terahertz MIMO antennas. Integrating graphene into MIMO antennas could improve key performance metrics such as bandwidth, radiation efficiency, and gain, which are crucial for 6 G applications [4].

Material advancements aside, accurate antenna performance and bandwidth prediction are a cornerstone in designing efficient MIMO systems [5]. Machine learning (ML) techniques have emerged as a potent tool in this context. By analyzing complex relationships between

* Corresponding author.
E-mail address: aateya@psu.edu.sa (A.A. Ateya).

https://doi.org/10.1016/j.rineng.2024.103216
Received 11 August 2024; Received in revised form 2 October 2024; Accepted 21 October 2024
Available online 23 October 2024

Table 1
Performance assessment of the proposed MIMO antenna compared to comparable research.

Ref	Operating range	BW (THz)	Substrate Material	Board Size (μm^2)	MIMO config.	Gain(dB)	Isolation (dB)	ECC, DG (dB)	Efficiency
[9]	0.51–0.78	0.27	Polyimide	600 × 600	–	9.19	–	–	90.84 %
[10]		0.11	Silicon dioxide	60 × 40	1 × 2	4.45	−25	0.0372, 9.99	–
[11]	0.72–2	2	Polyimide	125 × 125	2 × 2	8.2	−20	0.0022, 9.98	–
[12]	0.61–0.66	0.05	Polyimide	1200 × 2200	–	11.67	−25	0.003, 9.99	76.45 %
[13]	0.35–0.75	0.4	Polyimide	600 × 300	1 × 2	5.49	−25	0.015, 9.99	85.24 %
[14]	1.74–2.52	0.78	Polyamide	100 × 105	–	4.4	−20	0.006, 9.9998	–
[15]	0.093–0.207	0.114	Rogers RO4835-T	2000 × 1000	2 × 2	4.4	−17	0.006, 9.97	94 %
[16]	1.41–3	1.59	SiO_2	38 × 25	–	4.6	−25		74.5 %
This Work	0.631–4.962	4.331	Polyimide	95.52 × 227.24	1 × 2	13.3	−27	0.0002, 9.99	95 %

antenna characteristics and performance outcomes, these techniques offer a promising avenue for optimizing the design process, improving bandwidth prediction accuracy, and enabling a more efficient design space exploration compared to traditional methods [6]. This research aims to enhance the effectiveness of THz MIMO antennas using graphene and predict their bandwidth through machine learning analysis [7]. By incorporating graphene into antenna designs and utilizing advanced machine learning methods, this research seeks to improve THz MIMO antennas' performance and bandwidth limitations, thus facilitating their deployment in 6 G communication systems [8].

The advancements in THz communication, MIMO antennas, and their relevance to 6 G technology are well-documented in recent studies. For instance, the design in [9] utilizing a polyimide substrate operates within the 0.51–0.78 THz spectrum and boasts a bandwidth of 0.27 THz, its substantial 9.19 dB gain and 90.84 % efficiency are marred by the significant 600 × 600 μm^2 dimensions, limiting its use in compact devices. Furthermore, the absence of MIMO data is a notable drawback for contemporary systems, underscoring the need for a more versatile solution. The antenna in [10] functions within the frequency range of 1.76–1.87 THz, exhibiting a bandwidth of 0.11 THz and delivering robust MIMO performance (ECC 0.0372, DG 9.99) inside a compact design of 60 × 40 μm^2; nevertheless, its gain of 4.45 dB and restricted bandwidth present limitations. In [11], the 0.72–2 THz range exhibits an 8.2 dB gain and a 2 × 2 MIMO configuration, demonstrating commendable MIMO performance, notwithstanding −20 dB isolation. The antenna in [12] attains a gain of 11.67 dB; however, its substantial dimensions of 1200 × 2200 μm^2 and low efficiency restrict its use, albeit commendable MIMO isolation of −25 dB In [13], the 0.35–0.75 THz antenna, measuring 600 × 300 μm^2 and exhibiting a gain of 5.49 dB, demonstrates effective performance in MIMO; nonetheless, both gain and efficiency (85.24 %) require enhancement. The device in [14] functions within the frequency range of 1.74–2.52 THz, featuring a bandwidth of 0.78 THz, a modest gain of 4.4 dB, and an isolation level of −20 dB while also offering advantages due to its compact dimensions and effective MIMO performance. In [15], the 0.093–0.207 THz antenna demonstrates great efficiency (94 %) but is hindered by inadequate gain and isolation, rendering it unsuitable for MIMO systems in compact devices. The 1.41–3 THz antenna in [16] features a small design of 38 × 25 μm^2, exhibiting commendable MIMO performance; however, it is constrained by an efficiency of 74.5 %.

Table 1 shows a comparison between the suggested antenna's performance and the simulated outcomes of earlier research that has been published in the literature. The comparison demonstrates how the suggested design solves important issues such constrained bandwidth, decreased gain, and decreased efficiency, providing a more complete, high-performing solution appropriate for contemporary 6 G and THz communication systems. The suggested antenna functions across a frequency range of 0.631 to 4.962 THz, exhibiting a bandwidth of 4.331 THz, a gain of 13.3 dB, and an isolation of −27 dB This makes it an optimal choice for compact, contemporary devices, demonstrating superior MIMO performance (ECC 0.0002, DG 9.99) and an efficiency of 95 %. The proposed antenna has superior bandwidth, gain, and efficiency over other designs, offering a high-performance alternative for contemporary communication systems.

2. Research gap and contribution

The following is a synopsis of the most important contribution that this study makes:

This proposed effort entails analyzing the comparable RLC circuit of the proposed design, which must be incorporated into the previously mentioned literature. Ultimately, we achieved a high level of concordance between the results derived from the constructed equivalent circuit and those obtained from the simulation. When it comes to time and optimization, designing an antenna using traditional electromagnetic simulation tools like CST, HFSS, FEKO, or IE3D is no easy feat. These days, scientists are utilizing ML regression models to speed up the antenna design process and optimize the antenna's performance.

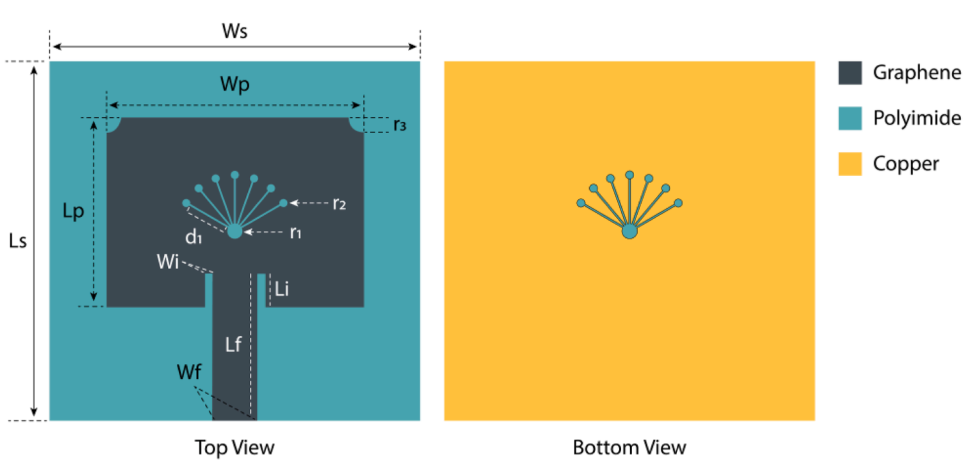

Fig. 1. Top and bottom view of the single-element antenna.

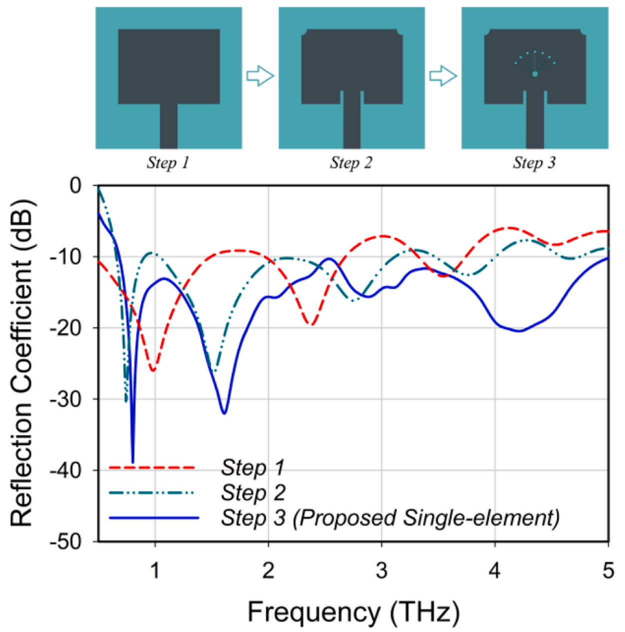

Fig. 2. Reflection Coefficient for different stages of single-element antenna.

Regression methods are the most effective approach for process optimization since their machine-learning evaluation is significantly faster than numerically solving a physical simulation model. You may also use regression models to determine how each design part contributed to the final product. Both the simulation and prediction outcomes are consistent. Regression methods are the most effective approach for process optimization since their machine-learning evaluation is significantly faster than numerically solving a physical simulation model.

3. Properties of graphene material

Graphene is a remarkable 2D material with a solitary layer of carbon atoms organized in a hexagonal configuration, creating a structure resembling a honeycomb [17]. It is a pure carbon allotrope, like graphite, carbon nanotubes, and fullerenes. However, unlike other carbon allotropes, graphene's unique properties make it an excellent conductor of electricity, with a high electron mobility that makes it well-suited for electronic applications. Graphene is typically regarded as chemically stable. However, its reactivity can be affected by the existence of defects or functional groups. The total conductivity of graphene depends on its chemical potential (μc) and relaxation time (τ). Specific parameters were chosen to design an efficient graphene antenna using CST. For instance, the temperature during the design process was set to 300 K. The chemical potential was fixed at μc=0.5 eV while the relaxation time was set to τ=1 ps. The antenna's lower frequency was set at 0.1 THz, and the higher frequency was 10 THz. Lastly, the thickness was set to 0.01 μm [18].

4. Different stages of designing a single-element antenna

Fig. 1 gives us the overall geometrical configuration of the proposed single-element antenna. Polyimide (εr = 3.5, thickness 10 μm) is used as a substrate, which is very suitable for the terahertz frequency range. The patch is rectangular and has a dimension of 68.62 × 50.52 μm^2 made of graphene. The patch is excited by inset-fed microstrip lines.

Fig. 2 depicts various stages of the single-element antenna and the frequency range of −10 dB for each stage. Initially, the antenna comprises a rectangular patch and a feedline. In the subsequent stage, two quarter circular-shaped slots with a radius of r3 μm were introduced at the top corners of the patch, along with two insets. Lastly, a complex slot in the centre of the patch, resembling the stigma of a Hibiscus flower, was created. Copper is utilized in the ground, featuring the same stigma-shaped slot as the patch [19].

Table 2
Antenna design parameters.

Parameter	Value (μm)	Parameter	Value (μm)	Parameter	Value (μm)
Ws	98.62	Lf	30	r2	1
Ls	95.52	Wi	2	r3	4
Wp	68.62	Li	9	d2	60
Lp	50.52	d1	12.05	Wm	227.24
Wf	12	r1	2		

For dimensions, our initial focus was on a primary patch antenna with a microstrip feed line, as demonstrated in Fig. 1. Our goal was to achieve resonance at a frequency of 1 THz (1000 GHz) by employing the mathematical Eqs. (1)-(5).

$$\lambda = \frac{c}{f} \tag{1}$$

Where λ represents the wavelength, the distance over which the wave's shape repeats. c represents the speed of light, which is approximately 3 × 10^8m s^{-1}. By applying Eq. (1), we determine that the value of λ is 300 μm. Polyimide's dielectric constant (ε_r), which serves as our substrate material, is 3.5. The thickness (h) is 10 μm.

$$\varepsilon_{\text{eff}} = \left(\frac{\varepsilon_r + 1}{2} + \frac{\varepsilon_r - 1}{2}\right) \times \left(1 + 12 \times \frac{h}{W}\right)^{-0.5} \tag{2}$$

By applying Eq. (2), we determine that the Effective Dielectric Constant, ε_{eff}, Is approximately equal to 2.83.

$$W = \frac{c}{2f} \times \sqrt{\frac{2}{\varepsilon_r + 1}} \tag{3}$$

Eq. (3) determines that the antenna's patch width. (W) is approximately 94.8 μm.

$$L = \frac{c}{\left(2f\sqrt{(\varepsilon_{\text{eff}})}\right)} - 2 \times \Delta L \tag{4}$$

$$\Delta L = 0.412h \times \frac{\frac{\varepsilon_{\text{eff}} + 0.3}{\frac{W}{h} + 0.264}}{\frac{\varepsilon_{\text{eff}} - 0.258}{\frac{W}{h} + 0.8}} \tag{5}$$

By employing Eqs. (4) and (5) with precision, we determine that the patch length (L) of the antenna is approximately 88.824 μm. We conducted detailed calculations to design an antenna that resonates at 1 THz or 1000 GHz frequency. The estimated data is slightly modified to obtain multiple resonance frequencies and a wider bandwidth.

Table 2 presents a comprehensive overview of the different diameters and their respective acronyms.

4.1. Analysis of the result of the single element by using graphene and copper

In the study of microstrip patch antennas, material selection for the patch and ground plane significantly impacts the antenna's performance [20]. Here, we analyse the results of using copper and graphene in various configurations to understand their effects on resonance frequency, bandwidth, return loss, and gain.

Fig. 3 shows the different configurations of the microstrip patch antenna using various materials for the patch and ground plane.

Fig. 4 compares the reflection coefficients for four possible configurations: a copper patch and ground plane, a patch and ground plane made of graphene, a copper patch with a graphene ground plane, and a graphene patch with copper ground. It also shows the gain for each configuration.

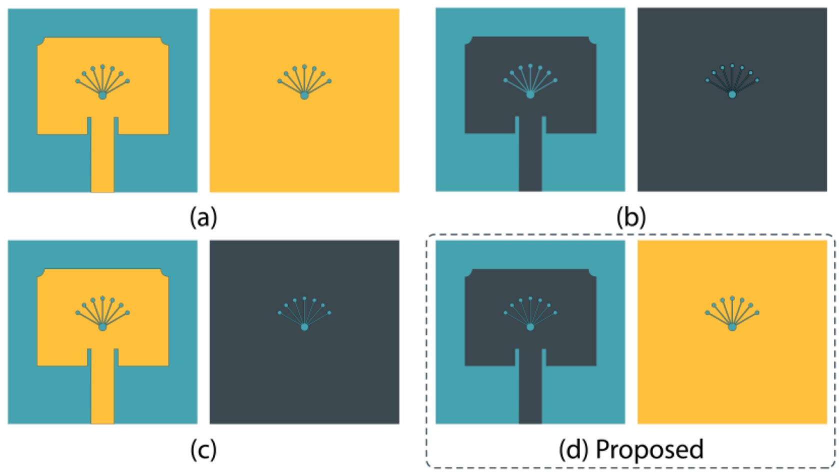

Fig. 3. (a) Copper-based patch and ground, (b) Graphene-based patch and ground, (c) Patch with copper and ground with graphene, (d) Patch with graphene and ground with copper.

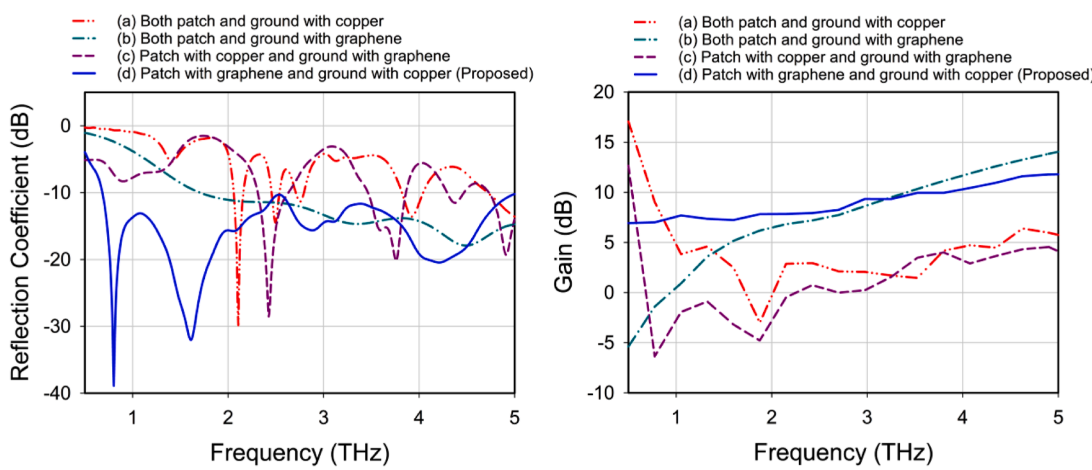

Fig. 4. A study of reflection coefficients and gain with varied ground and patch material combinations.

When both the patch and ground plane are copper, the antenna resonates at one frequency, but the bandwidth is very narrow, limiting the operational frequency range. The gain in this setup is low, which can impact signal strength and range.

Using graphene for both the patch and ground plane achieves higher gain, indicating better radiation efficiency and stronger signals. However, the absence of any specific resonance frequency and a higher return loss make it unusable.

With a copper patch and graphene ground plane, it shows relatively better reflection coefficient properties. It has three resonance frequencies but a lower gain.

The final configuration, with a graphene patch and copper ground plane, shows excellent reflection coefficient properties. This setup balances the benefits of both materials, potentially offering wide bandwidth and good gain.

5. MIMO configuration

Terahertz communication functions within the ultrahigh-frequency spectrum, providing the possibility of much-increased data transmission rates compared to conventional communication frequencies. MIMO (Multiple-Input Multiple-Output) is employed to enhance the capacity of a radio link by utilizing transmit and receive antennas to exploit multipath propagation. This is a solution to the problem of data rate limitation encountered by single-input-single-output (SISO) systems. MIMO is employed to enhance the channel's capacity, increase the system's reliability, and optimize the transmission of data by employing the maximum capacity of wireless communication systems [21].

Fig. 5 depicts the aerial and underneath perspectives, whereas Fig. 6 illustrates the three-dimensional representation of the MIMO antenna we have put forth. This is a 1 × 2 MIMO antenna with the identical substrate length as a single element but an increased width of Wm μm. A distance of d2 μm separates the patches.

However, a primary concern in MIMO antenna design is enhancing antenna performance while maintaining a compact size. When the antennas are positioned nearby, the radiation from one antenna disturbs the others, resulting in a drop in antenna performance. To attempt to solve this problem, we have implemented a graphene barrier between the individual element antennas [22]. The barrier is composed of polyimide, the same material as the substrate. The wall has a height of 20 μm and a width of 10 μm. We applied a graphene layer to both sides of the wall [23].

6. Result of MIMO antenna

6.1. Reflection and transmission coefficient

The reflection coefficient is a vital measure for evaluating the performance of a microstrip patch antenna. A decreased reflection

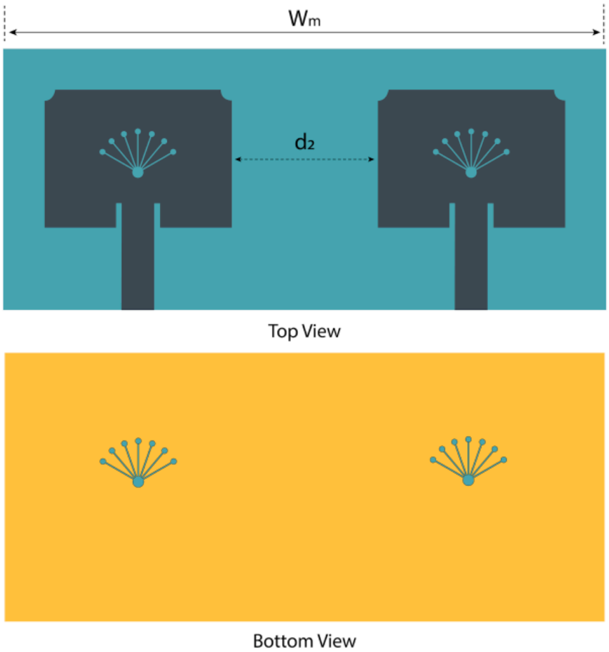

Fig. 5. Top and bottom view of the proposed MIMO antenna.

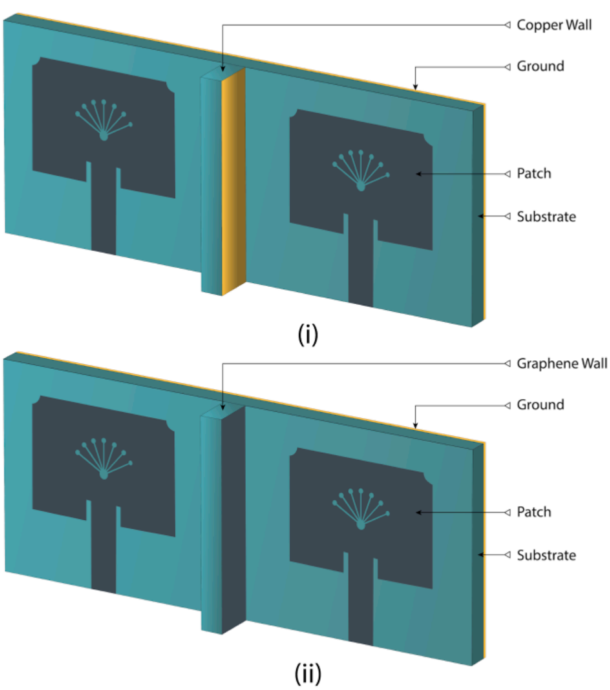

Fig. 6. 3-dimensional view of the proposed MIMO antenna. (i) Copper Wall (ii) Graphene Wall.

coefficient ensures optimal power transfer from the feed line to the antenna, resulting in higher radiation and improved antenna efficiency [24].

Fig. 7 depicts the different antenna reflection coefficients, showcasing contrasting responses in the absence of a wall compared to the presence of walls made of different materials. Based on the diagram, the antenna demonstrates resonance at a frequency of 0.8 THz and a lower return loss of −40 dB without any barriers, while the antenna's bandwidth is 4.27 THz, from 0.68 THz to 4.95 THz. However, the reflection coefficient exhibits significant variation when introducing a copper-

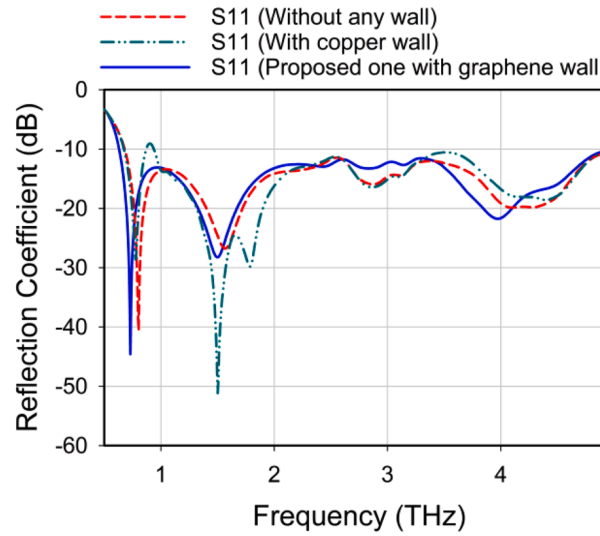

Fig. 7. Exploring wall impact on MIMO antenna: Reflection coefficients without and with Graphene/Copper walls.

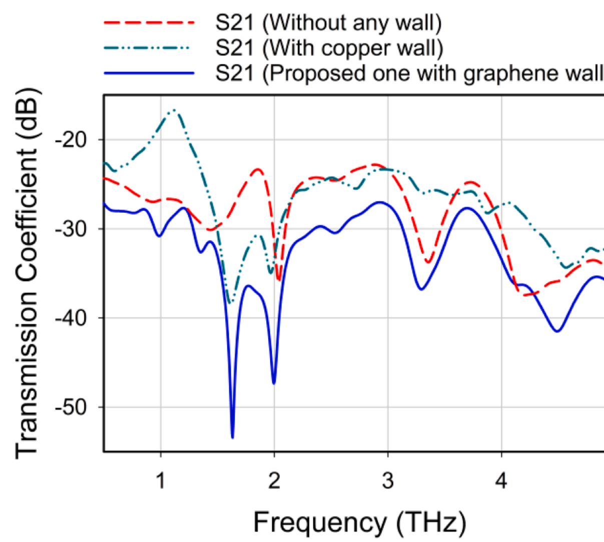

Fig. 8. Exploring wall impact on MIMO antenna: Transmission coefficients without and with Graphene/Copper walls.

material barrier between the antenna elements. Subsequently, the Reflection coefficient is altered to 1.5 THz, and the bandwidth became 4 THz (0.94–4.94 THz). Substituting the copper with graphene material (proposed) enhanced the antenna's isolation performance. The resonance frequency shifts to 0.73 THz, with a return loss of −44.7 dB The bandwidth is 4.331 and spans from 0.631 THz to 4.962 THz.

The degree of independence between the antenna elements, a crucial factor in assessing the performance of the MIMO antenna, is of paramount importance. The transmission coefficient, which measures this degree, evaluates the extent to which each antenna can send or receive signals without interference from its neighbors. This underscores the gravity of the issue in MIMO antenna performance assessment.

Fig. 8 shows that when no wall is present, the isolation between the antennas is observed to be −22 dB This low isolation, which could interfere with signals coming from one another, is a significant concern as it can lead to a decrease in the system's performance. A further reduction in isolation to −18 dB occurs with introducing the copper wall between the antenna elements. However, antenna performance improvements were demonstrated by replacing copper with graphene.

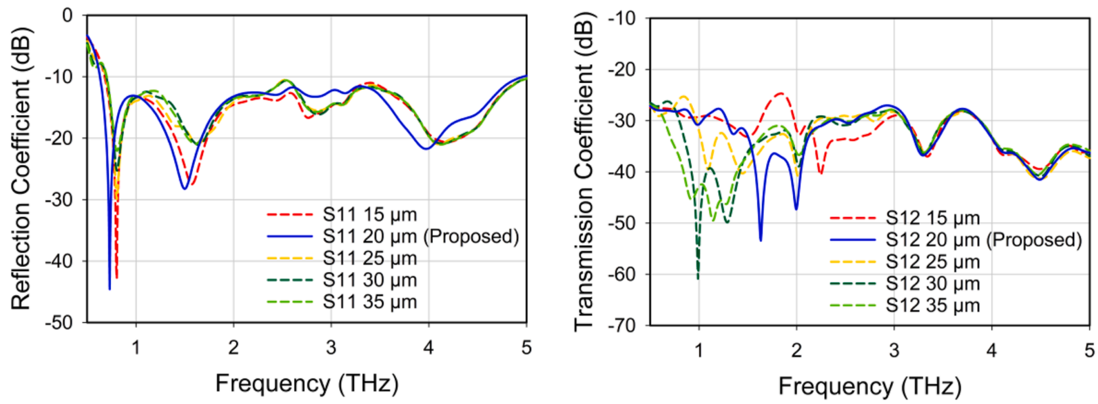

Fig. 9. Implementing different heights of decoupling wall and analysing the result.

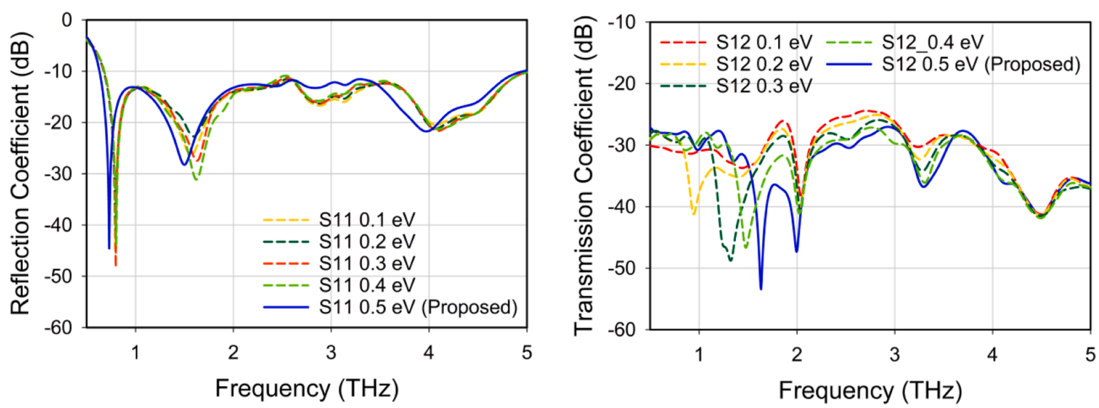

Fig. 10. analysis of the result of the antenna based on various chemical potentials.

After that, the antenna demonstrates a high isolation of −27 dB, which enables a more distinct isolation of the streams that are being sent.

When comparing several situations, the arrangement of the graphene wall showed the most desirable outcomes in terms of bandwidth, reflection, and transmission coefficient. This result indicates that the presence of a graphene wall enhances the antenna's versatility and adaptability to various communication standards.

6.1.1. Reflection and transmission coefficient for different wall height

Fig. 9 presents the analysis of reflection and transmission coefficients for various wall heights in the context of antenna performance. The wall heights explored in this study are 15 µm, 20 µm, 25 µm, 30 µm, and 35 µm. These wall heights' corresponding return loss values are −42.5 dB, −45 dB, −29.92 dB, −25.25 dB, and −22.03 dB, respectively. This shows that as the wall height increases, there is a noticeable degradation in return loss, indicating a reduction in the effectiveness of signal reflection at higher wall heights. Conversely, the isolation values, representing the ability of the wall to decouple signals, are reported as −24.6 dB, −27 dB, −25.24 dB, −26.18 dB, and −27.93 dB The findings suggest that the wall height impacts the isolation less linearly, with 20 µm and 35 µm walls exhibiting slightly improved isolation characteristics.

6.1.2. Reflection and transmission coefficient for different chemical potential of graphene

In Fig. 10, the reflection and transmission coefficients for various graphene chemical potentials are studied. The chemical potentials examined are 0.1 eV, 0.2 eV, 0.3 eV, 0.4 eV, and 0.5 eV The return loss values recorded for these potentials are −44.67 dB, −41.44 dB, −48.19 dB, −43.79 dB, and −45 dB Notably, the return loss at 0.3 eV presents the highest value, indicating optimal performance in reducing signal reflection. The isolation values for the respective chemical potentials are −24.3 dB, −25.07 dB, −25.75 dB, −26.98 dB, and −27 dB, with a gradual improvement in isolation as the chemical potential increases. These results provide insights into how altering graphene's chemical potential can fine-tune the antenna's performance, particularly in optimizing isolation and return loss.

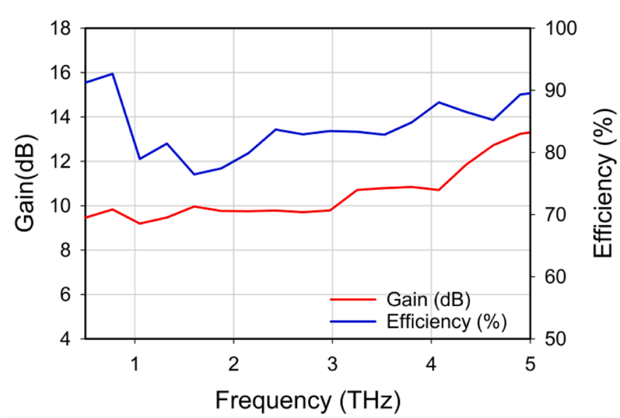

Fig. 11. Gain and efficiency of the proposed MIMO antenna.

6.2. Gain and efficiency

To properly evaluate the antenna's performance, it is essential to comprehend and effectively optimize the gain. Gain, a measurement of how well the antenna can focus and direct the energy that it either transmits or receives, is a crucial performance metric. Higher gain levels

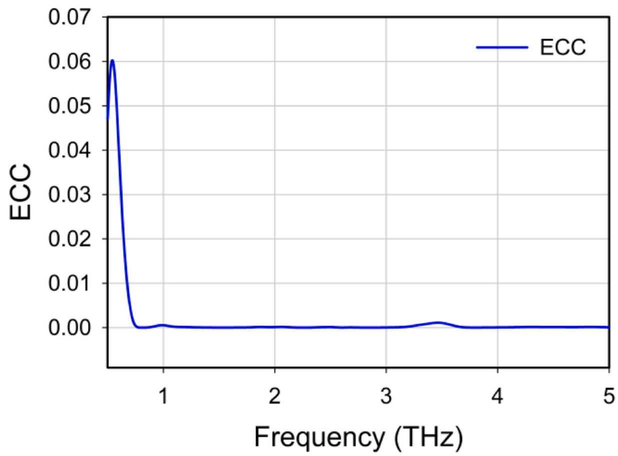

Fig. 12. Simulated ECC of the proposed MIMO antenna.

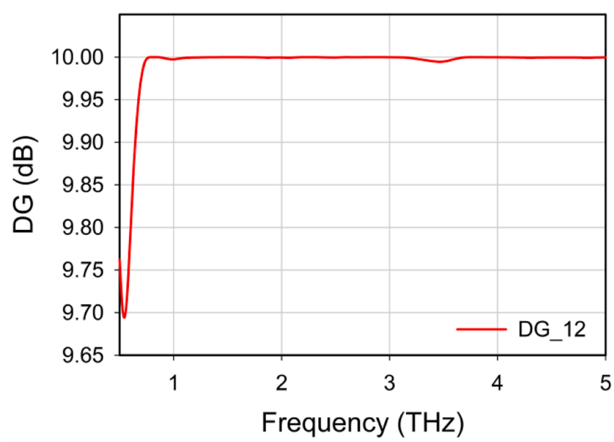

Fig. 13. Simulated DG of the proposed MIMO antenna.

imply that the beam is more focused and the signal is more robust in the intended direction [25]. Radiation efficiency, another important performance metric, represents the proportion of the input power transferred as radio waves [26].

Fig. 11 depicts the proposed work's simulated gain and suggested radiation efficiency. The figure makes it abundantly evident that the antenna has a high radiation efficiency of 95 % and a peak gain of 13.3 dB, suggesting that it can effectively convert the input power into the energy directed from the antenna.

6.3. Envelop correlation coefficient (ECC)

Envelop Correlation Coefficient (ECC) plays a vital role in evaluating the effectiveness of antennas in MIMO systems, which utilize numerous antennas to improve data transmission speeds and reliability. The ECC is a quantitative measure employed to assess the level of similarity between the radiation patterns of two antennas. Generally, a number near zero or <0.5 is favorable for MIMO systems, as it signifies improved diversity performance and decreased signal degradation caused by correlation [27].

The antenna shown in Fig. 12 has an envelope correlation Coefficient (ECC) of 0.0002 dB throughout the working frequency range.

Calculates the ECC, a vital metric laboring to evaluate the indentation of similarity among radiation patterns generated by different antennas.

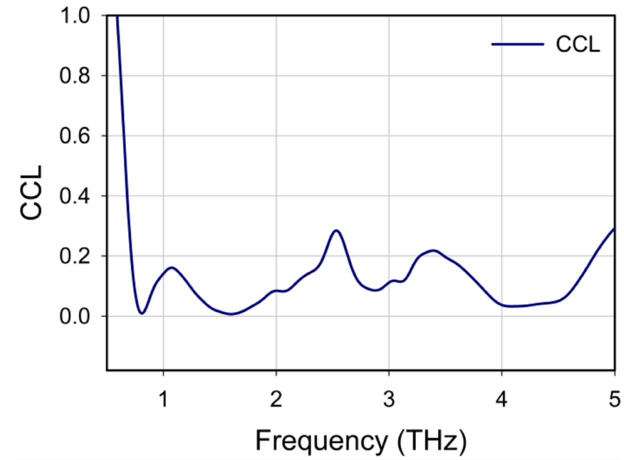

Fig. 14. CCL of proposed MIMO antenna.

$$ECC = \frac{\left|\int_{4\pi}[E_1(\theta,\varphi) * E_2(\theta,\varphi)]d\Omega\right|^2}{\int_{4\pi}|E_1(\theta,\varphi)|^2 d\Omega \int_{4\pi}|E_2(\theta,\varphi)|^2 d\Omega} \quad (6)$$

6.4. Diversity gain (DG)

When assessing the performance of MIMO antennas, diversity gain (DG) must be considered a significant metric. Diversity gain quantifies the enhancement in a communication system's efficiency when employing numerous antennas in the presence of fading or other unfavorable channel circumstances [28]. The following equation can determine the magnitude of DG in a MIMO system.

$$DG = 10\sqrt{1 - ECC^2} \quad (7)$$

Fig. 13 demonstrates that the simulated value of DG is 9.99, resulting in enhanced communication that is both dependable and robust.

6.5. Channel capacity loss (CCL)

Channel Capacity Loss (CCL) is a key parameter for MIMO antenna efficiency. Measure the Channel Capacity Limit to see if a channel can transfer data uninterrupted. MIMO system channel capacity grows proportionally with antenna element count. Correlation between MIMO channels causes capacity losses. MIMO channel capacity must be measured using the CCL or Channel Capacity Loss when there is a correlation. This can be determined using Eq. (8) [29].

$$CCL = -\log_2 \det(p_R) \quad (8)$$

The receiver two-port correlation matrix can be calculated using Eq. (9).

$$p_R = \begin{pmatrix} \rho_{xx} & \rho_{xy} \\ \rho_{yx} & \rho_{yy} \end{pmatrix} \quad (9)$$

Where,

$$\rho_{xx} = 1 - \left(|S_{xx}|^2 + |S_{xy}|^2\right)$$

$$\rho_{yy} = 1 - \left(|S_{yy}|^2 + |S_{yx}|^2\right)$$

$$\rho_{xy} = \left|S_{xx}^* S_{xy} + S_{yx}^* S_{xy}\right|^2$$

$$\rho_{yx} = \left|S_{yy}^* S_{yx} + S_{xy}^* S_{yx}\right|^2$$

The ports 1 and 2 coefficients are (x) and (y). <0.5 bps/Hz is recommended for CCL. See Fig. 14 for the appropriate antenna's Channel Capacity Loss, most like CCLs below 0.4 bps/Hz. Simulation and experimental results show that the suggested antenna's Channel

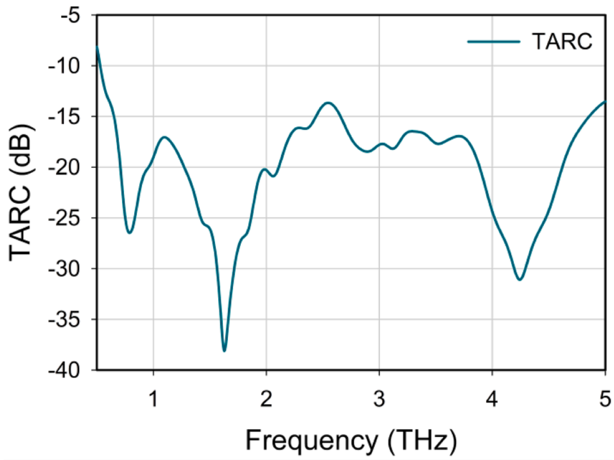

Fig. 15. TARC of proposed MIMO antenna.

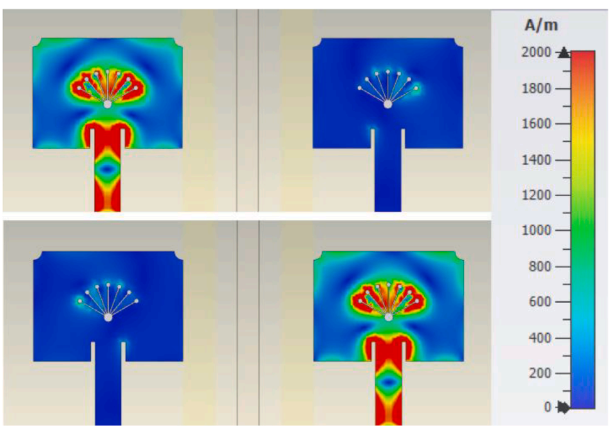

Fig. 16. Current Distribution of Proposed MIMO Antenna.

Capacity Loss (CCL) is 0.3 bps/Hz across the operational frequency range.

6.6. *Total active reflection coefficient (TARC)*

TARC, or Total Active Reflection Coefficient, is important in four-port antennas because it shows the relationship between sent and received power. Eq. (10) can determine this [30].

$$TARC = \frac{\sqrt{(|S_{xx}| + |S_{xy}|)^2 + (|S_{yx}| + |S_{yy}|)^2}}{\sqrt{4}} \tag{10}$$

The ideal Total Active Reflection Coefficient (TARC) for MIMO antennas is <0 dB. Fig. 15 shows the proposed antenna's simulated TARC outputs of <−10 dB.

6.7. *Current distribution*

Antenna current distribution is how electricity flows along the length of an antenna. The way current flows through an antenna is a big part of its radiation pattern, impacting how well it works [31].

Fig. 16 shows the surface currents at 3 THz for the MIMO antenna with one excited port and matched loads at the other ports. The most crucial surface current, at 2000 A m^{-1}, comes from the feedline near insets and a stigma-shaped slot.

6.8. *Radiation pattern*

The radiation pattern can evaluate the antenna's performance, which shows how the power is spread out in different directions [32]. The antenna is usually in the central position of the polar coordinates picture, which shows the azimuth, or horizontal direction, on the x-axis.

The simulated and observed 2D radiation patterns for the electric (E field) and magnetic (H field) fields are shown in Fig. 17. The primary lobe magnitude in the E-field at $\varphi = 0°$ is 11.8 dBV/m, and the 3 dB angular beam width at $\varphi = 90°$ is 94.1° On the other hand, the electric field pattern (E Field) has a primary lobe magnitude of 12 dBV/m at an angle of theta 90° at 3 THz.

Regarding magnetic (H field), at $\varphi = 0°$, the primary lobe magnitude is −47.3 dBA m^{-1}, and the 3 dB angular beam width is 58.1° at $\varphi = 90°$. The magnetic field pattern (H Field) has a primary lobe magnitude of −40.1 dBA m^{-1} when theta is 90°.

7. Result and analysis for equivalent circuit in ADS vs CST simulation tools

This section examines the resonant frequency and bandwidth of the proposed MIMO antenna using lumped circuit components. The resonant frequency produced by the antenna structure is determined by R, L, and C elements, as the conductive materials create resistance, inductance, and capacitance. These properties are represented through an equivalent circuit model [33]. By analyzing the antenna's impedance in CST simulations, we extracted the R, L, and C values and used them to calculate the impedance. As a result, the lumped element equivalent circuit was developed using Agilent ADS.

Fig. 18 presents the lumped element model, incorporating resistors, inductors, and capacitors, accurately reflecting the operational characteristics of the proposed MIMO antenna.

To refine the initial model, we employed a trial-and-error approach using ADS software, iteratively adjusting the RLC parameters to align the circuit's response with the simulation results from the full-wave electromagnetic model. This process involved fine-tuning each parameter to replicate the impedance, resonance, and overall performance of the antenna components. The patch, responsible for two resonant frequencies, was modeled using a parallel circuit of resistance (R1), capacitance (C1), and inductance (L1). Additionally, the stigma slot at the center of the patch is represented by creating a series circuit consisting of capacitance (C2) and inductance (L2). Multiple such series circuits are then combined to form a more intricate and complex circuit, accurately capturing the electrical behavior of the stigma slot and effectively modeling its characteristics within the overall antenna structure. The feedline was accurately modeled with resistance (R2), capacitance (C4), and inductance (L4), capturing its electrical characteristics. For the graphene layer of both sides of the polyamide wall, a parallel circuit of L3 and C3 was introduced. By integrating these circuit elements, we constructed a model that closely mirrored the behavior of the MIMO antenna. The R-l-C circuit model was simulated using Agilent ADS to confirm its equivalence to the actual antenna design.

To ensure accuracy, we compared the CST simulation results with those of the equivalent circuit model, focusing on the S11 parameter. Fig. 18 illustrates this comparison, providing a detailed evaluation of the R-l-C circuit model's ability to accurately replicate the antenna's behavior.

Fig. 19 compares the results of the CST simulation with a similar circuit simulation using the return loss. The simulation result shows that the center frequency is 0.73 THz, with an impedance bandwidth of 4.331 THz and a return loss level of −44.7 dB The R, L, and C equivalent circuits demonstrate resonance at a frequency of 0.68 THz. The device has an impedance bandwidth of 3.98 THz and a return loss level of −39 dB The results indicate a favorable correlation between the resonant frequency and the extent of return loss.

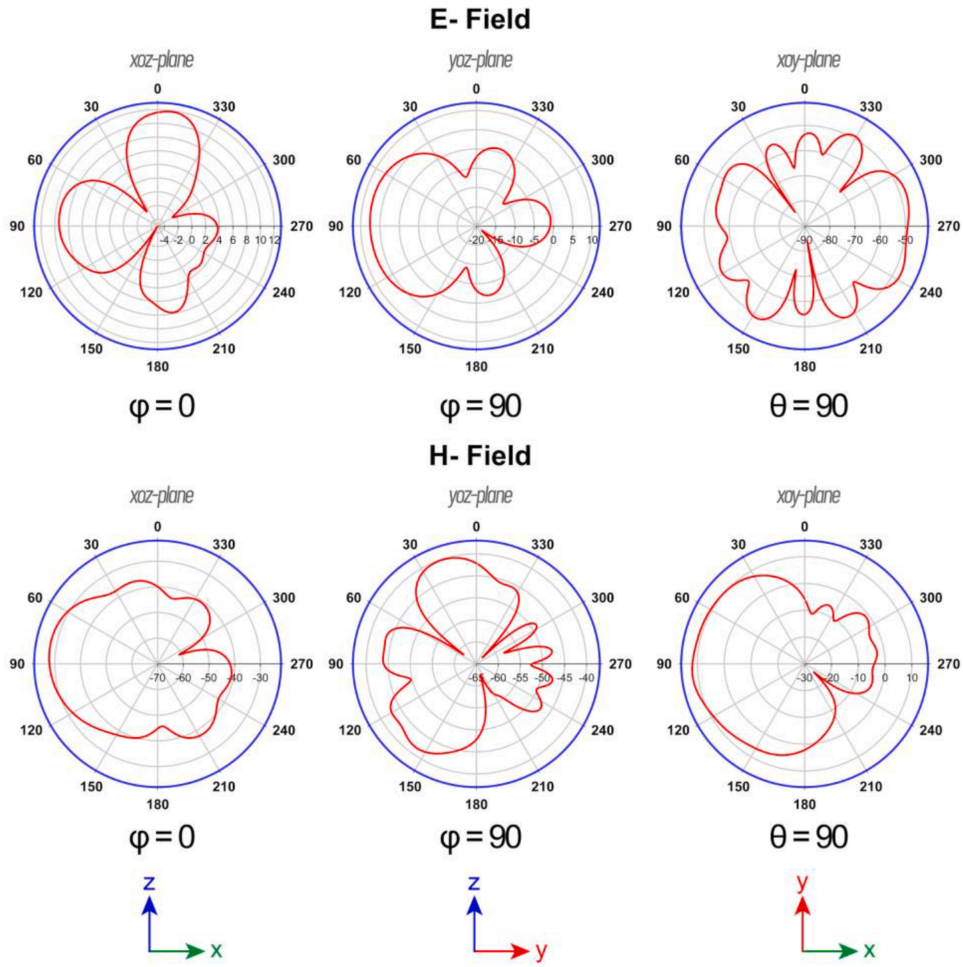

Fig. 17. Simulated Radiation Pattern of Proposed MIMO Antenna.

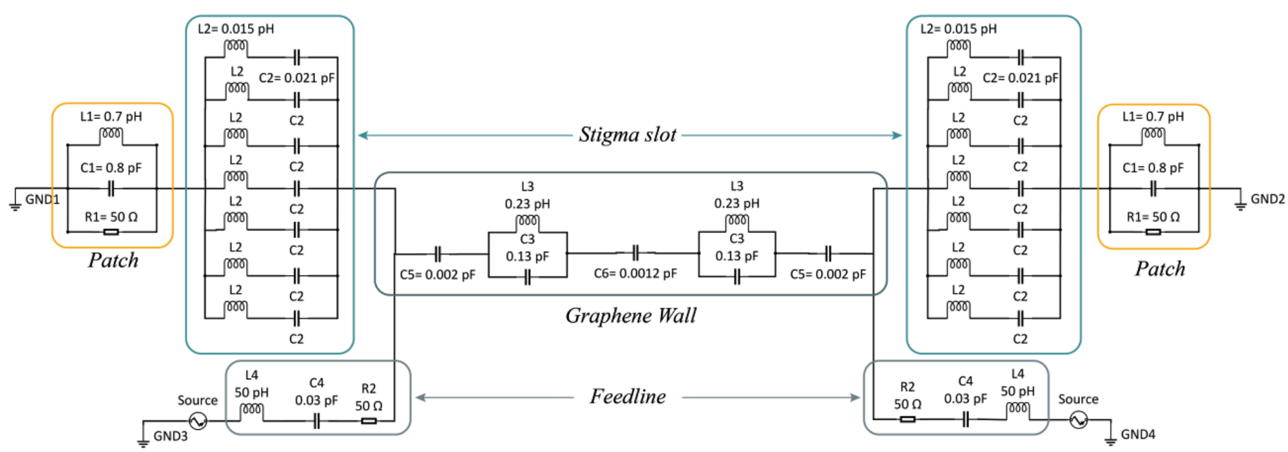

Fig. 18. Circuit model for the proposed MIMO Antenna.

8. Machine learning (ML) analysis

Designing an antenna utilizing commercial electromagnetic modeling tools, such as CST, HFSS, FEKO, and IE3D, is highly demanding due to the time and optimization requirements involved. Designing an antenna with minimal dimensions and acceptable antenna outputs is highly laborious and time-consuming. Furthermore, the situation becomes more intricate when distinct slots are located on the upper part of the patch and the ground plane. Researchers are utilizing machine learning (ML) regression models to accelerate the antenna design process and enhance antenna performance. Utilizing machine learning simplifies the process of forecasting antenna size for desired outputs or vice versa. ML algorithms can scour various antenna configurations in search of the optimal values for various performance metrics, including gain, bandwidth, and radiation pattern. Faster iteration and evaluation of various antenna designs are made possible by ML's ability to automate the process of investigating new design combinations. By using this strategy instead of the more conventional trial-

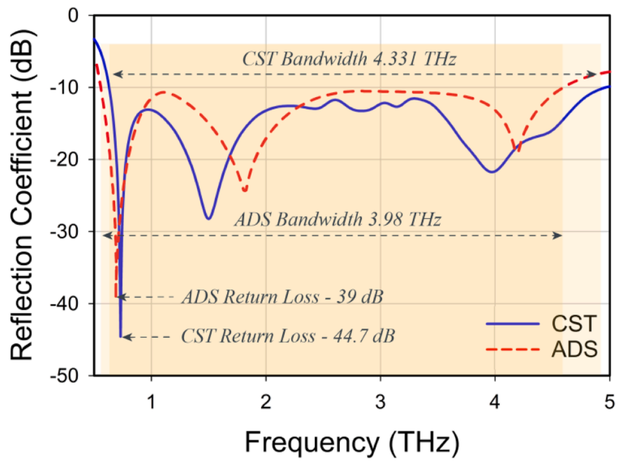

Fig. 19. Reflection coefficient disparity between CST and ADS for MIMO antenna.

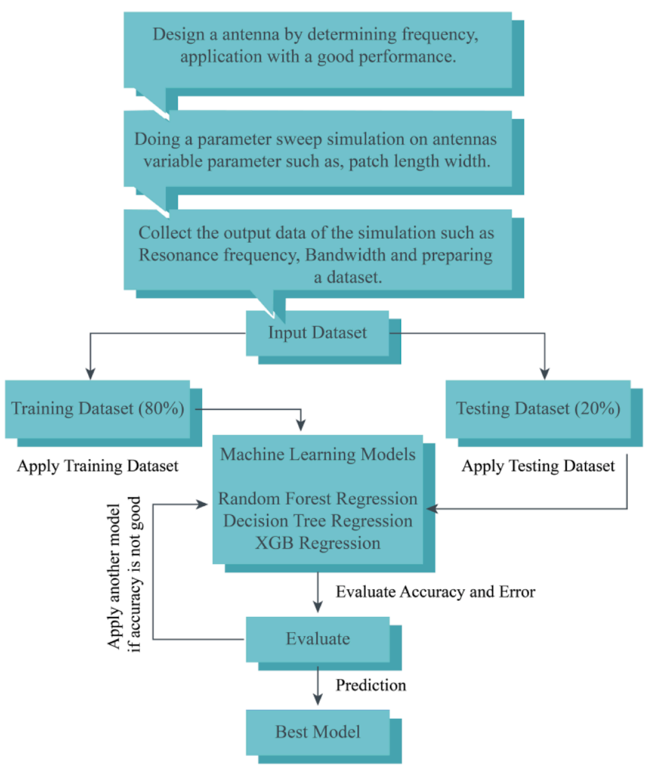

Fig. 20. Diagram illustrating the sequential process involved in the development of machine learning.

and-error approach, time and resources can be saved. With ML models, designers can make educated decisions regarding antenna performance based on different design criteria before physically constructing and testing prototypes [34].

8.1. Result and analysis for machine learning

The ML approach comprises two components. Commence by utilizing the simulation tool CST to fabricate a THz MIMO antenna. These parameters are used to extract parameters of relevance, such as resonance frequency, bandwidth, impedance matching, or radiation efficiency. Using parametric sweeps, investigate how the antenna's performance is affected by various design characteristics. Determine the optimal methodology using machine learning model training on the given dataset. After collecting 90 data points, we estimate the bandwidth using multiple regression machine learning. This is done after modelling the proposed antenna using the CST simulation tool. During the training phase, 80 % of the data is utilized, while the remaining 20 % is reserved for evaluation reasons, as depicted in Fig. 20. The dimensions of the substrate (length, breadth, and height) and the dimensions of the feed (length and width) are the input variables in our dataset. Upon completing the training and validation process, the model can predict various outputs, such as bandwidth.

8.1.1. Gaussian process regression (GPR)

One non-parametric Bayesian method for solving regression problems is the Gaussian Process (GP) regression. It is an effective method for simulating interdependent, non-linear connections. Compared to parametric models, GP regression models the entire distribution over functions rather than assuming a fixed functional form for the connection.

8.1.2. XGB regression

For regression using XGBoost, the standard procedure is to prepare the data, adjust the model's hyperparameters, train it on a training dataset, and then use it to forecast fresh data. Perfect for regression issues, the model learns to convert input features into continuous output values. XGBoost has been successful in many domains, including healthcare, finance, and data science contests [35].

8.1.3. Bayesian linear regression

A probabilistic method for linear regression that applies Bayesian concepts is known as Bayesian linear regression. Conventional linear regression uses point estimates, like maximum likelihood estimates, to determine the model's parameters. Bayesian linear regression allows us to describe uncertainty and produce probabilistic predictions by treating the parameters as random variables with probability distributions [36].

8.1.4. Random forest regression

Random Forest is a versatile ensemble learning technique that may be utilized for both classification and regression applications. Random Forest Regression is the term used in the context of regression. The Random Forest algorithm theories plentiful decision trees throughout the training process and produces the average forecast (in the case of regression) each tree makes [37].

8.1.5. Ridge regression

When avoiding overfitting or dealing with linear regression problems involving numerous correlated characteristics, Ridge Regression proves to be an invaluable tool. Unlike other regularization approaches, Ridge Regression does not lead to precisely zero coefficients, making it less effective for feature selection even if it supports coefficient shrinkage [38].

8.1.6. Decision tree regression

Machine learning algorithms like Decision Tree Regression are helpful for regression challenges. Although decision trees are more often linked with classification, they can be modified to execute regression by forecasting a continuous value for the output rather than a label. Decision Tree Regression can calculate the output by repeatedly dividing the input space into regions and giving each region a fixed value (usually the median or mean) [39].

8.2. Performance measurement metrics

Performance evaluation measures for regression models are utilized to determine the degree to which a model is accurate in predicting the values of a continuous outcome variable. These measures help evaluate the accuracy, precision, and complete performance of the model [40].

An essential measure for assessing the efficacy of a regression model is the Mean Absolute Error (MAE), calculated as the average absolute

Table 3
Performance metrics for bandwidth prediction.

Algorithm/ Regression	MAE	MSE	RMSE	R2	EVS
Gaussian Process	0.26 %	0.18 %	0.34 %	99.30 %	98.84 %
XGB Regressor	0.70 %	0.90 %	1.08 %	91.29 %	92.48 %
Bayesian Linear	0.35 %	0.17 %	0.41 %	90.00 %	91.00 %
Random Forest	0.34 %	0.37 %	0.60 %	86.68 %	85.68 %
Ridge Regressor	0.86 %	0.21 %	1.05 %	78.09 %	79.11 %
Decision Tree	0.75 %	0.31 %	1.03 %	82.43 %	83.43 %

difference between the actual and predicted values. It gives a measure of the typical error magnitude, which is independent of whether the errors are overestimated or underestimated. A lower MAE number signifies a more effective model. The formula for MAE is as follows:

$$MAE = \frac{1}{n}\sum_{i=1}^{n}|y_i - \hat{y}_i| \tag{11}$$

Where, n = number of errors and $|Pi - Oi|$ = absolute error

The Mean Squared Error (MSE) is a widely employed statistic for evaluating the effectiveness of a regression model. It quantifies the average squared disparities between predicted and actual values. It measures the average squared difference between the predictions made by the model and the actual results. Smaller Mean Squared Error (MSE) values imply superior model performance [41]. MSE can be calculated using the expression:

$$MSE = \frac{1}{n}\sum_{i=1}^{n}(y_i - \hat{y}_i)^2 \tag{12}$$

Regression model performance metrics like Root Mean Squared Error (RMSE) are commonly used to evaluate prediction accuracy. Relative Mismatch Error (RMSE) is a variant of Mean Squared Error (MSE) that takes the square root of the sum of all squared differences amongst the actual and projected values [42].

$$RMSE = \sqrt{\frac{1}{n}\sum_{i=1}^{n}(Pi - Oi)^2} \tag{13}$$

R-squared (R^2), or the coefficient of determination, is a statistical metric that quantifies the proportion of the variability in the dependent variable that the independent variables can account for in a regression model. The evaluation of the blimey of fit of a regression model is often

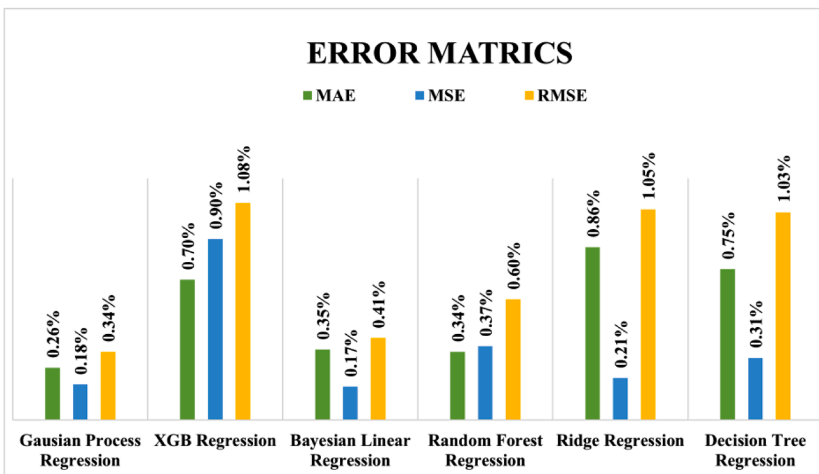

Fig. 21. Error matrix Bar Chart for Gaussian Process Regression.

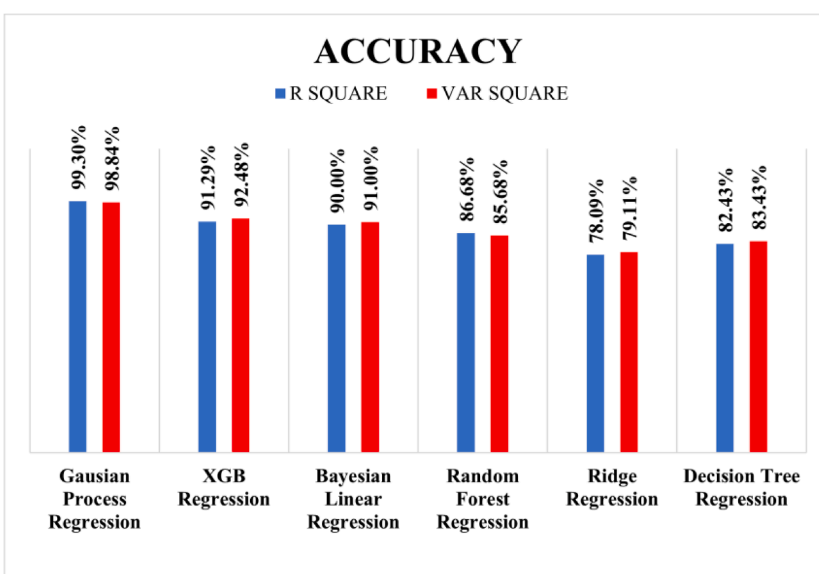

Fig. 22. Accuracy comparative Bar Chart for Gaussian Process Regression.

Table 4
Simulated and predicted bandwidth using Gaussian Process Regression.

No	Simulated BW	Predicted BW	No	Simulated BW	Predicted BW
1	4.33671	4.337599	10	4.33099	4.3111
2	4.347749	4.34782	11	4.63865	4.6183
3	4.33174	4.331795	12	4.33155	4.3316
4	4.22568	4.2256	13	4.36045	4.3504
5	4.33177	4.3518	14	4.33036	4.3304
6	4.3131	4.3131	15	4.32694	4.3270
7	4.33184	4.3320	16	4.66442	4.6641
8	4.3462	4.3461	17	4.32779	4.3278
9	4.33166	4.3317	18	4.43718	4.4373

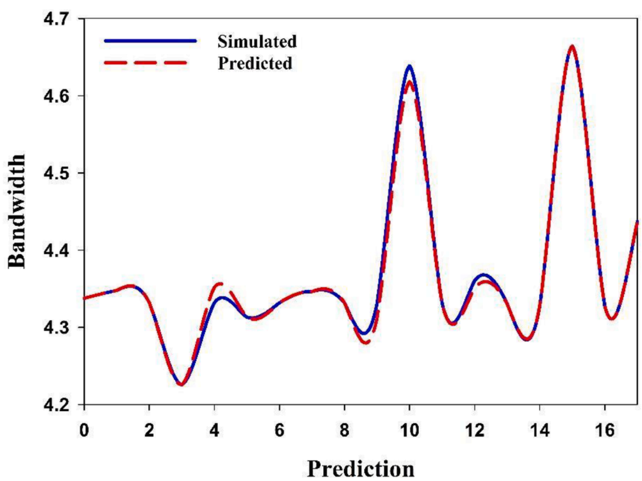

Fig. 23. Simulated vs predicted bandwidth using Gaussian Process Regression.

done using this metric [43].

$$R^2 = 1 - \frac{\sum_{i=1}^{N}(y_i - \widehat{y}_i)^2}{\sum_{i=1}^{N}(y_i - \widehat{y}_i)^2} \tag{14}$$

The explained variance score quantifies the fraction of the variance in the dependent variable that the model can account for. The range of values is from 0 to 1. When the explained variance is 0, it means no variance is explained. The model does not account for any variation. The explained variation equals 1, indicating that the model accounts for all variations [44].

$$explained\ variance\ (y, \widehat{y}) = 1 - \frac{Var(y - \widehat{y})}{Var(y)} \tag{15}$$

The effectiveness metrics for predicting bandwidth are shown in Table 3. Multiple necessary measures show that the "Gaussian Process Regression" model performs best. The Minimum Absolute Error (MAE) was 0.26 %, the Minimum Squared Error (MSE) was 0.18 %, and the Maximum Root Mean Squared Error (RMSE) was 0.34 %, as shown in Fig. 21. Moreover, " Gaussian Process Regression" has an impressive R-squared (R^2) value of 99 % and a remarkable Var Score of 99 %, highlighting its ability to explain a substantial part of the variation shown in Fig. 22.

The data in Table 4 shows little difference (very close to zero) between the actual and predicted levels of efficiency for the Gaussian Process Regression model. Furthermore, the mistake rate is usually <1 % [45]. Fig. 23 shows a strong link between these numbers and the model's predicted efficiency. Based on its better results in predicting efficiency compared to other ML models, Gaussian Process Regression was chosen.

9. Conclusion

THz band MIMO antennas is designed for 6 G applications. Bandwidth predictions are made using several regression model methodologies. The initial MIMO design in CST exhibits a remarkable efficiency rating of 95 %, a maximum gain of 13.3 dB, and an impressive isolation measurement exceeding 27. These results indicate the high potential for success in this design. Additional validation of the CST results was obtained by replicating the same RLC circuit in the ADS using a functionally equivalent model. Results with reflection coefficients like those obtained from the CST and ADS simulators are accessible. Subsequently, it assesses its effectiveness by utilizing several machine-learning techniques. Gaussian process regression exhibits outstanding precision, achieving an accuracy of over 99 %, as seen by the elevated R-square and var scores. In addition, it attains the most minimal error rates when forecasting bandwidth, with a mean absolute error (MAE) of 0.26 %, a mean squared error (MSE) of 0.18 %, and a root mean squared error (RMSE) of 0.34 %. The efficiency calculations and projections conducted using Gaussian Process Regression indicate that this antenna is an optimal model for future 6 G applications.

CRediT authorship contribution statement

Md Ashraful Haque: Investigation, Formal analysis, Conceptualization. **Redwan A. Ananta:** Conceptualization, Methodology, Investigation, Software, Writing – original draft. **Jamal Hossain Nirob:** Writing – original draft, Visualization. **Md. Sharif Ahammed:** Writing – original draft, Software, Methodology. **Narinderjit Singh Sawaran Singh:** Supervision, Resources. **Liton Chandra Paul:** Writing – review & editing, Writing – original draft, Visualization. **Abeer D. Algarni:** Funding acquisition. **Mohammed ElAffendi:** Validation, Supervision, Software. **Abdelhamied A Ateya:** Project administration, Investigation.

Declaration of competing interest

All authors have no conflicts of interest.

Funding

This research was funded by Princess Nourah bint Abdulrahman University Researchers Supporting Project number (PNURSP2024R51), Princess Nourah bint Abdulrahman University, Riyadh, Saudi Arabia.

Acknowledgements

This research was acknowledged by Princess Nourah bint Abdulrahman University, Riyadh, Saudi Arabia. Also, the authors would like to acknowledge the support of Prince Sultan University, Riyadh, Saudi Arabia. The author also would like to acknowledge the support of Daffodil International University, Bangladesh.

Data availability

Data will be made available on request.

References

[1] H. Wang, et al., High-performance transparent ultrabroadband electromagnetic radiation shielding from microwave toward terahertz, ACS Appl. Mater. Interfaces 15 (42) (2023) 49487–49499, https://doi.org/10.1021/acsami.3c10474. Oct.
[2] Z. Zheng, Y. Zhang, L. Shi, L. Wu, J.-F. Mao, An overview of probe-based millimeter-Wave/Terahertz far-field antenna measurement setups [Measurements Corner], IEEE Antennas Propag. Mag. 63 (2) (2021) 63–118, https://doi.org/10.1109/MAP.2021.3054017. Apr.
[3] I.F. Akyildiz, C. Han, Z. Hu, S. Nie, J.M. Jornet, Terahertz band communication: an old problem revisited and research directions for the next decade, IEEE Trans. Commun. 70 (6) (Jun. 2022) 4250–4285, https://doi.org/10.1109/TCOMM.2022.3171800.

[4] A.L. Imoize, O. Adedeji, N. Tandiya, S. Shetty, 6G Enabled smart infrastructure for sustainable society: opportunities, challenges, and research roadmap, Sensors 21 (5) (2021) 1709, https://doi.org/10.3390/s21051709. Mar.

[5] R. Krishan, Performance analysis of terahertz microstrip antenna designs: a review, in: R. Rawat, R.K. Chakrawarti, S.K. Sarangi, R. Choudhary, A.S. Gadwal, V. Bhardwaj (Eds.), Robotic Process Automation, 1st ed., Wiley, 2023, pp. 101–112, https://doi.org/10.1002/9781394166954.ch6.

[6] Y. Lu, X. Zheng, 6G: a survey on technologies, scenarios, challenges, and the related issues, J. Ind. Inf. Integr. 19 (Sep. 2020) 100158, https://doi.org/10.1016/j.jii.2020.100158.

[7] M. Banafaa, et al., 6G mobile communication technology: requirements, targets, applications, challenges, advantages, and opportunities, Alex. Eng. J. 64 (2023) 245–274, https://doi.org/10.1016/j.aej.2022.08.017. Feb.

[8] L. Ismail, R. Buyya, Artificial intelligence applications and Self-Learning 6G networks for smart cities digital ecosystems: taxonomy, challenges, and future directions, Sensors 22 (15) (2022) 5750, https://doi.org/10.3390/s22155750. Aug.

[9] A. Hocini, M.N. Temmar, D. Khedrouche, M. Zamani, Novel approach for the design and analysis of a terahertz microstrip patch antenna based on photonic crystals, Photonics Nanostructures - Fundam. Appl. 36 (2019) 100723, https://doi.org/10.1016/j.photonics.2019.100723. Sep.

[10] G. Varshney, S. Gotra, V.S. Pandey, R.S. Yaduvanshi, Proximity-coupled two-port multi-input-multi-output graphene antenna with pattern diversity for THz applications, Nano Commun. Netw. 21 (2019) 100246, https://doi.org/10.1016/j.nancom.2019.05.003. Sep.

[11] S. Das, D. Mitra, S.R. Bhadra Chaudhuri, Fractal loaded planar super wide band four element MIMO antenna for THz applications, Nano Commun. Netw. 30 (2021) 100374, https://doi.org/10.1016/j.nancom.2021.100374. Dec.

[12] R. Pant, L. Malviya, Terahertz MIMO antenna array for future generation of wireless applications, Frequenz 0 (0) (2024), https://doi.org/10.1515/freq-2023-0203. Feb.

[13] K.V. Babu, S. Das, G.N.J. Sree, B.T.P. Madhav, S.K.K. Patel, J. Parmar, Design and optimization of micro-sized wideband fractal MIMO antenna based on characteristic analysis of graphene for terahertz applications, Opt. Quantum Electron. 54 (5) (2022) 281, https://doi.org/10.1007/s11082-022-03671-2. May.

[14] A. Kumar, D. Saxena, P. Jha, N. Sharma, Compact two-port antenna with high isolation based on the defected ground for THz communication, Results Opt 13 (2023) 100522, https://doi.org/10.1016/j.rio.2023.100522. Dec.

[15] T. Okan, High efficiency unslotted ultra-wideband microstrip antenna for sub-terahertz short range wireless communication systems, Optik (Stuttg) 242 (2021) 166859, https://doi.org/10.1016/j.ijleo.2021.166859. Sep.

[16] K.V. Babu, G.N.J. Sree, T. Islam, S. Das, M.E. Ghzaoui, R.A. Saravanan, Performance analysis of a photonic crystals embedded Wideband (1.41–3.0 THz) fractal MIMO antenna over sio2 substrate for terahertz band applications, Silicon 15 (18) (2023) 7823–7836, https://doi.org/10.1007/s12633-023-02622-0. Dec.

[17] M. Li, et al., Graphene: preparation, tailoring, and modification, Exploration 3 (1) (2023) 20210233, https://doi.org/10.1002/EXP.20210233. Feb.

[18] K. Moradi, A. Pourziad, S. Nikmehr, Characteristic mode analysis of graphene-based patch antenna in terahertz regime, Arab. J. Sci. Eng. (2024), https://doi.org/10.1007/s13369-023-08580-4. Feb.

[19] K.V. Babu, P.C. Shifali, J. Manisha, G.D. Bhavani, G.N.J. Sree, Design and implementation of MIMO graphene patch antenna to improve isolation for THz applications, Microsyst. Technol. 29 (10) (2023) 1443–1453, https://doi.org/10.1007/s00542-023-05536-4. Oct.

[20] S.N.H. Sa'don, M.H. Jamaluddin, A. Althuwayb, B. Alali, A review: the influence of graphene material integration in antenna characteristics in the presence of bias for fifth and sixth generation wireless communication application, Nano Commun. Netw. 39 (2024) 100483, https://doi.org/10.1016/j.nancom.2023.100483. Mar.

[21] M.A. Rahman, S.S. Al-Bawri, W.M. Abdulkawi, K. Aljaloud, M.T. Islam, A unique SWB multi-slotted four-port highly isolated MIMO antenna loaded with metasurface for IOT applications-based machine learning verification, Eng. Sci. Technol. Int. J. 50 (2024) 101616, https://doi.org/10.1016/j.jestch.2024.101616. Feb.

[22] Md.M. Hasan, M.T. Islam, T. Alam, A. Alzamil, M.S. Soliman, Electromagnetic coupling shielding in compact MIMO antenna using symmetric T-shaped metamaterial structure for 5G communications, Opt. Laser Technol. 169 (2024) 110046, https://doi.org/10.1016/j.optlastec.2023.110046. Feb.

[23] N.K. Maurya, S. Kumari, P. Pareek, L. Singh, Graphene-based frequency agile isolation enhancement mechanism for MIMO antenna in terahertz regime, Nano Commun. Netw. 35 (2023) 100436, https://doi.org/10.1016/j.nancom.2023.100436. Mar.

[24] M.A. Haque, L.C. Paul, S. Kumar, R. Azim, Md.S. Hosain, M. Azman Zakariya, A Plowing T-shaped patch antenna for WiFi and C Band Applications, in: 2021 International Conference on Automation, Control and Mechatronics for Industry 4.0 (ACMI), IEEE, Rajshahi, Bangladesh, Jul. 2021, pp. 1–4, https://doi.org/10.1109/ACMI53878.2021.9528266.

[25] L.C. Paul, M.A. Haque, M.A. Haque, M.M.U. Rashid, M.F. Islam, M.M. Rahman, Design a slotted metamaterial microstrip patch antenna by creating three dual isosceles triangular slots on the patch and bandwidth enhancement. 2017 3rd International Conference on Electrical Information and Communication Technology (EICT), 2017, pp. 1–6, https://doi.org/10.1109/EICT.2017.8275143. Khulna, Bangladesh.

[26] Md.A. Haque, M.A. Zakariya, L.C. Paul, D. Nath, P. Biswas, R. Azim, Analysis of slotted E-shaped microstrip patch antenna for Ku band applications, in: 2021 IEEE 15th Malaysia International Conference on Communication (MICC), IEEE, Malaysia, 2021, pp. 98–101, https://doi.org/10.1109/MICC53484.2021.9642100. Dec.

[27] A. Abbas, et al., Highly selective multiple-notched UWB-MIMO antenna with low correlation using an innovative parasitic decoupling structure, Eng. Sci. Technol. Int. J. 43 (Jul. 2023) 101440, https://doi.org/10.1016/j.jestch.2023.101440.

[28] A. Baz, D. Jansari, S.P. Lavadiya, S.K. Patel, Miniaturized and high gain circularly slotted 4×4 MIMO antenna with diversity performance analysis for 5G/Wi-Fi/WLAN wireless communication applications, Results Eng 20 (2023) 101505, https://doi.org/10.1016/j.rineng.2023.101505. Dec.

[29] Md.A. Haque, et al., Broadband high gain performance MIMO antenna array for 5 G mm-wave applications-based gain prediction using machine learning approach, Alex. Eng. J. 104 (2024) 665–679, https://doi.org/10.1016/j.aej.2024.08.025. Oct.

[30] S.S. Al-Bawri, et al., Machine learning technique based highly efficient slotted 4-port MIMO antenna using decoupling structure for sub-THz and THz 6G band applications, Opt. Quantum Electron. 56 (10) (2024) 1611, https://doi.org/10.1007/s11082-024-07249-y. Sep.

[31] Md.A. Haque, L.C. Paul, R. Azim, Md.M. Mowla, A. Saleh, Md.N. Hossain, A Modified E-Shaped Microstrip Patch Antenna for C Band Satellite Applications, in: 2019 IEEE International Conference on Signal Processing, Information, Communication & Systems (SPICSCON), IEEE, Dhaka, Bangladesh, 2019, pp. 27–31, https://doi.org/10.1109/SPICSCON48833.2019.9065126. Nov.

[32] L.C. Paul, M.S. Akhter, M.A. Haque, M.R. Islam, M.F. Islam, M.M. Rahman, Design and analysis of four elements E, H and combined E-H shaped microstrip patch array antenna for wireless applications, in: 2017 3rd International Conference on Electrical Information and Communication Technology (EICT), IEEE, Khulna, 2017, pp. 1–6, https://doi.org/10.1109/EICT.2017.8275141. Dec.

[33] Md.A. Haque, et al., Quasi-Yagi antenna design for LTE applications and prediction of gain and directivity using machine learning approaches, Alex. Eng. J. 80 (2023) 383–396, https://doi.org/10.1016/j.aej.2023.08.059. Oct.

[34] Md.A. Haque, et al., Dual band antenna design and prediction of resonance frequency using machine learning approaches, Appl. Sci. 12 (20) (2022) 10505, https://doi.org/10.3390/app122010505. Oct.

[35] S.R. Shakya, M. Kube, Z. Zhou, A comparative analysis of machine learning approach for optimizing antenna design, Int. J. Microw. Wirel. Technol. (Aug. 2023) 1–11, https://doi.org/10.1017/S1759078723001009.

[36] H. Zhao, Y. Ding, L. Meng, Z. Qin, F. Yang, A. Li, Bayesian multiple linear regression and new modeling paradigm for structural deflection robust to data time lag and abnormal signal, IEEE Sens. J. 23 (17) (2023) 19635–19647, https://doi.org/10.1109/JSEN.2023.3294912. Sep.

[37] D. Borup, B.J. Christensen, N.S. Mühlbach, M.S. Nielsen, Targeting predictors in random forest regression, Int. J. Forecast. 39 (2) (2023) 841–868, https://doi.org/10.1016/j.ijforecast.2022.02.010. Apr.

[38] Y. Zheng, et al., New ridge regression, artificial neural networks and support vector machine for wind speed prediction, Adv. Eng. Softw. 179 (2023) 103426, https://doi.org/10.1016/j.advengsoft.2023.103426. May.

[39] Md.A. Haque, et al., Machine learning-based technique for resonance and directivity prediction of UMTS LTE band quasi Yagi antenna, Heliyon 9 (9) (Sep. 2023) e19548, https://doi.org/10.1016/j.heliyon.2023.e19548.

[40] Md.A. Haque, et al., Machine learning-based technique for gain and resonance prediction of mid band 5G Yagi antenna, Sci. Rep. 13 (1) (2023) 12590, https://doi.org/10.1038/s41598-023-39730-1. Aug.

[41] M. Ashraful Haque, et al., Machine Learning-Based Approach for bandwidth and frequency Prediction for N77 band 5G Antenna, Phys. Scr. 99 (2) (2024) 026005, https://doi.org/10.1088/1402-4896/ad1d40. Feb.

[42] P. Takyi-Aninakwa, S. Wang, H. Zhang, Y. Xiao, C. Fernandez, A NARX network optimized with an adaptive weighted square-root cubature Kalman filter for the dynamic state of charge estimation of lithium-ion batteries, J. Energy Storage 68 (2023) 107728, https://doi.org/10.1016/j.est.2023.107728. Sep.

[43] K. Taira, D. McInnes, L. Zhang, How many data points and how large an R-squared value is essential for Arrhenius plots? J. Catal. 419 (2023) 26–36, https://doi.org/10.1016/j.jcat.2023.01.033. Mar.

[44] D. Iacobucci, D.L. Popovich, S. Moon, S. Román, How to calculate, use, and report variance explained effect size indices and not die trying, J. Consum. Psychol. 33 (1) (2023) 45–61, https://doi.org/10.1002/jcpy.1292. Jan.

[45] Md.K. Ahmed, et al., based performance estimation of a slotted inverted F-shaped tri-band antenna for satellite/mm-wave 5G application, TELKOMNIKA Telecommun. Comput. Electron. Control 22 (4) (2024) 773, https://doi.org/10.12928/telkomnika.v22i4.26028. Aug.